SLPcalculator: a web-based tool to estimate nanoparticle heating with peak analysis and F -test

LÓPEZ-VÁZQUEZ, Iago <http://orcid.org/0009-0008-7371-5679>, FERNÁNDEZ-AFONSO, Yilian <http://orcid.org/0000-0002-0970-1917>, SANTANA-OTERO, Antonio <http://orcid.org/0000-0002-2204-4093>, RUTA, Sergiu <http://orcid.org/0000-0001-8665-6817>, AMIGO, Alfredo, MORALES, M. Puerto <http://orcid.org/0000-0002-7290-7029>, CHANTRELL, Roy W. <http://orcid.org/0000-0001-5410-5615>, GUTIÉRREZ, Lucía <http://orcid.org/0000-0003-2366-3598> and SERANTES, David <http://orcid.org/0000-0002-3860-2133>

Citation:

Copyright and re-use policy

Check for updates

SLPcalculator: a web-based tool to estimate nanoparticle heating with peak analysis and *F*-test

Iago López-Vázquez, [a,b] Yilian Fernández-Afonso, [c,d] Antonio Santana-Otero, [a] Sergiu Ruta, [e] Alfredo Amigo, [a] M. Puerto Morales, [d] Roy W. Chantrell, [f] Lucía Gutiérrez *[c] and David Serantes *[a,b]

Accurately determining the Specific Loss Power (SLP) remains a major challenge in magnetic hyperthermia and photothermal heating. In this work, we examine the practical implementation of the Peak Analysis Method (PAM), an alternative to Newton's-law-based approaches. Our focus is on how the number of data points affects the identification of the linear regime around the peak of the $\Delta T(t)$ curve, as this method relies on calculating and comparing the slopes of the heating and cooling branches around the maximum. Using an *F*-test-based statistical criterion, we objectively determine the valid linear range and compare the resulting SLP values with those obtained from the Initial Slope Method (ISM), one of the most common Newton-law-based approaches, which also relies on linear range fit. Our results reveal that the correct determination of the linear range leads to significantly different SLP values compared to those obtained using arbitrary time windows, underlining the necessity of employing statistical criteria for a robust and reproducible analysis. Finally, we introduce an open-access website (SLPcalculator.com) that integrates PAM with the *F*-test, providing a systematic and user-friendly tool for reliable SLP estimation without the need for manual fitting procedures.

1. Introduction

The SLP (Specific Loss Power) is a fundamental parameter used to characterize the capacity of nanoparticles (NPs) to produce heat when subjected to external stimuli, either an alternating magnetic field -in the case of magnetic hyperthermia-, or a laser -in the case of photothermal therapy. Despite its central role for comparison of different materials, or to support proper determination of the heating conditions for a specific application, it is widely accepted that there is a huge variation in SLP values determined using different experimental setups.[1] Some of the problems that lead to such variability arise from the inhomogenous temperature profiles[2,3] but also from the coexistence of different heat diffusion mechanisms.[4] These are strongly related to the heat-loss mechanisms characteristic of a given experimental apparatus. Essentially these lead to non-adiabatic behaviour, and time-dependent

temperature profiles, resulting in deviations from Newton's law of cooling.[5,6] These factors contribute to errors which vary between instruments. Moreover, in addition to these uncertainties, the heat production may be time-dependent due to colloidal evolution during the hyperthermia experiments,[7–9] which adds further complexity to the problem.

To address this important issue, in a previous work we developed a new protocol to characterize the SLP value from the peak of the temporal evolution of the temperature curve, $\Delta T(t)$, around the switch on/off field point.[6] The key postulate of our alternative approach to the problem is that, irrespective of the spatial temperature profile and its dynamics, it is essentially the same during heating and cooling phases close to the peak. As will be shown later this peak analysis method (PAM) allows to compensate for the heating losses leading to a more correct value of the SLP. Briefly, the PAM procedure consists of obtaining the SLP value from linear fits of the $\Delta T(t)$ curve before and after the peak; since both would correspond to the same temperature profile, its actual shape would not play a role (see ref. 6 for further details). Note that, thus far, the methodology summary did not refer specifically to magnetic hyperthermia nor to photothermia, which reflects its generality to study either phenomenon.

This new approach has several advantages. Firstly, it allows the rapid production of a series of peaks (Zigzag protocol[6]) that allows calculation of the error associated with the SLP

[a]Applied Physics Department, Universidade de Santiago de Compostela, Spain.
E-mail: david.serantes@usc.es
[b]Instituto de Materiais (iMATUS), Universidade de Santiago de Compostela, Spain
[c]Instituto de Nanociencia y Materiales de Aragón (INMA, UNIZAR-CSIC) and
CIBER-BBN, Spain. E-mail: lu@unizar.es
[d]Instituto de Ciencia de Materiales de Madrid (ICMM-CSIC), Spain
[e]College of Business, Technology and Engineering, Sheffield Hallam University, UK
[f]School of Physics, Electronics and Technology, The University of York, York, UK
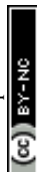
determination faster than repeating measurements to analyze, for example, the initial slope several times. Furthermore, it allows us to calculate the SLP at different global temperatures or after exposure of the particles to the field for different amounts of time. In the case of a system with a time-dependent SLP (for example because of chaining of magnetic NPs (MNPs) under AC fields[9,10]), this allows determination of the time dependence of the SLP. However, as noted in ref. 6, this requires accurate determination of the experimental error to give confidence in the presence of a time dependent SLP. The reliable determination of the SLP and associated error is the main aim of this work.

In this respect, while the theoretical basis of the PAM is complete and robust, there are some aspects that need further study. In particular, the optimum number of data points representing the trade-off between resolution and accuracy needs to be analyzed. Since the peak analysis is theoretically ascribed to the peak (i.e. the smaller $\Delta(T)$ range around it, the better), it is equivalent to say that it has the same restriction (in terms of data points) as the initial slope method (ISM). Since in essence the numerical determination is analogous to the ISM, but with two slopes instead of one, one could think that the additional uncertainty due to subtracting two slopes could give a poorer SLP value. A key objective to determine here is whether the theoretically more solid background of the PAM approach can compensate such higher uncertainty due to using two slopes. Furthermore, we aim to elucidate rigorously the data range within which the temperature behaves *linearly* with time.

In this work, we have studied the SLP value as a function of the number of data points for standard magnetic hyperthermia experiments, but it is noted the results should be also applicable to photothermia, as previously described. For completeness and based on its relevance for the literature, as it is commonly used, we have compared the values with those obtained from the initial slope approach. Our aim is to establish an optimal protocol for data analysis using the peak analysis method, so the community working on magnetic hyperthermia characterization has available a robust technique that minimizes the variability found in the literature until now. Central to our investigation is the use of statistical methods to determine the optimal trade-off between the size of the time measurement interval and the significance of non-linearity on the fit. Finally, as a part of this work, we have developed a python-based analyser which has been released as a web-based application for community use (SLPcalculator.com). Beyond extending the original PAM protocol, the present work introduces a quantitative statistical framework to assess the accuracy and robustness of SLP determination. By incorporating an objective criterion to select the optimal time interval for linear fitting, this approach not only improves the precision of the PAM but also enhances the reliability of commonly used methods such as the initial slope method. Importantly, the proposed statistical analysis is general and can be readily applied to other calorimetric approaches for SLP evaluation.

The article is organised as follows: first, in section 2 details of the experiments are described, together with a brief summary of the PAM and a description of the *F*-test statistical analysis. Then, the results are reported in section 3, including an in-depth analysis of the linear range identification and the role of measurement repetition on accuracy. Subsequently, in section 4 we introduce SLPcalculator.com, the free software we have developed and made publicly available to provide statistically significant SLP determination. Finally, the main conclusions are summarised in section 5.

2.   Materials and methods

2.1.   Magnetic nanoparticles synthesis and characterization

Iron oxide octahedral nanoparticles were selected as a reference material that has been used in our previous work.[6] Briefly, particles were prepared through an oxidative precipitation aqueous route based on a synthesis previously reported[11] but with minor modifications. A solution of $FeSO_4$ (1 M) was prepared in 50 mL of H_2SO_4 0.01 M. This liquid was then added to a solution composed of $NaNO_3$ (4.25 g), NaOH (4.22 g), water (137 mL) and ethanol (63 mL, 96% vol). The mixture resulted in a green rust suspension that was stirred for 15 min and then placed on a thermostatic bath at 90 °C for 6 hours. The prepared particles, were then subjected to an acid treatment and subsequently coated with dextran.[12] The main characteristics of these particles were already reported.[6] Briefly, transmission electron microscopy (TEM) confirmed the particle shape and an average size of 32.0 ± 6.7 nm. Field dependent magnetization at 300 K recorded in a SQUID magnetometer yielded saturation magnetization of ≈ 77 Am^2 $kg_{Fe_3O_4}^{-1}$; remanent magnetization of ≈ 12 Am^2 $kg_{Fe_3O_4}^{-1}$ and coercive field values of ≈ 4 kA m^{-1}, in agreement with literature values for magnetite/maghemite nanoparticles.

2.2.   Magnetic hyperthermia measurements

The magnetic hyperthermia measurements, comprising the time dependent temperature variation, were performed using a Fives Celes 12, 118 M01 generator. For the measurements, 1 ml of a suspension with an iron concentration of 1 mg mL^{-1} in water was placed in a plastic microtube. The microtube was located at the centre of the magnetic induction coil inside an insulating holder and the temperature was monitored until a stable temperature was reached before turning the AC magnetic field on. The AC field conditions used were 166 kHz and 25 mT.

The AC field was applied for either 1, 2 or 4 minutes, and the temperature variation was recorded during heating and the subsequent cooling. Temperature was recorded with an OSENSA fiber optic probe (PRB-G40-02 M-STM-MRI). These measurements were repeated 10 times for each of the different heating times.

2.3.   Peak analysis method (PAM)

The foundation of the PAM was described in detail in ref. 6. A brief summary is provided below.

The basis of our approach is that the system temporal and spatial evolution is accurately described by the heat diffusion equation:

$$\rho_r c_r \frac{\partial \Delta T_r}{\partial t} = k_r \frac{\partial^2 \Delta T_r}{\partial r^2} + S_0, \qquad (1)$$

where $\Delta T_r = T_r - T_{env}$, ρ stands for density, c for heat capacity, k for thermal conductivity, and S_0 is the heat source term. The subscript "r" refers to the spatial dependence, and "env" denotes the environment.

Without loss of generality, we may write eqn (1) to describe both the heating and cooling parts of a typical magnetic hyperthermia $\Delta(T)(t)$ curve, as

$$\left[\frac{\partial \Delta T_r}{\partial t}\right]_{heating} = \alpha_r \left[\frac{\partial^2 \Delta T_r}{\partial r^2}\right]_{heating} + S, \qquad (2)$$

for the heating part, and

$$\left[\frac{\partial \Delta T_r}{\partial t}\right]_{cooling} = \alpha_r \left[\frac{\partial^2 \Delta T_r}{\partial r^2}\right]_{cooling}. \qquad (3)$$

for the cooling one. Both in eqn (2) and (3), $\alpha_r = k_r/\rho_r c_r$ and $S = S_0/\rho_r c_r$. In our previous work[6] we showed that the spatial derivatives of both equations are the same in the limit of the transition between heating and cooling stages, i.e. at the peak of the $\Delta T(t)$ curve. Thus, at the peak one can obtain the S value (and therefore the SLP) by subtracting both equations, giving:

$$S = \left[\frac{\partial \Delta T_r}{\partial t}\right]_{heating} - \left[\frac{\partial \Delta T_r}{\partial t}\right]_{cooling}. \qquad (4)$$

Eqn (4) clearly shows that the SLP, included within the "S" parameter as

$$SLP = S \cdot \frac{\left(\frac{\rho_{NP}}{C} - 1\right)\rho_w c_w + \rho_{NP} c_{NP}}{\rho_{NP}}, \qquad (5)$$

is in this way determined *independently of the actual temperature distribution of the experiment*, thereby removing an important device-dependent factor. In eqn (5), ρ and c correspond to density and specific heat of the nanoparticles (NP) and embedding medium (w refers to water); C stands for the nanoparticle concentration.

2.4. Statistical analysis

As derived in our previous work[6] and summarized in the preceding section, the PAM was implemented by performing linear fits to the heating and cooling branches of the $\Delta T(t)$ curve, immediately before and after the ON/OFF switching of the applied field. The slopes extracted from both sides of the peak were then combined to evaluate the S parameter as given by eqn (4). A similar linear fitting procedure was also applied within the framework of the Initial Slope Method (ISM).

2.4.1. Linear range determination. When performing these linear fits, it is important to determine whether the data can indeed be described by a straight line, or whether additional curvature should be taken into account. To address this issue, we employed the F-test, a statistical procedure commonly used to compare two nested models, i.e., a simpler one and a more complex one that includes an additional parameter.[13,14] The F-test evaluates whether the reduction in the chi-squared value achieved by the additional parameter is statistically significant.[15] In our case, the simple model corresponds to the linear fit, while the more complex one includes an additional quadratic term. The F-statistic is defined as:[15]

$$F_x = \frac{\chi^2(m) - \chi^2(m+1)}{\chi^2(m+1)/(N-m-1)} = \frac{\Delta\chi^2}{\chi^2(m+1)/(N-m-1)}, \qquad (6)$$

where $\chi^2(m)$ is the chi-squared value of the simpler model with m free parameters, $\chi^2(m+1)$ is that of the more complex model including an additional parameter, and N is the total number of data points. In our case, $m = 2$ (slope and intercept for the linear fit). To determine whether the additional term significantly improves the model, we compared the calculated value F_x with the critical value F_{crit} of the F-distribution table at a chosen significance level, accepting the simpler linear model when $F_x < F_{crit}$.

In our analysis, we considered a significance level of $\alpha = 0.05$, which indicates a 5% probability of rejecting the null hypothesis when it is actually true. In other words, there is a 5% risk of concluding that the additional term improves the model fit when it does not.

2.4.2. Repeated measurements and averaging. As stated previously, several independent measurements were performed for different heating times to obtain a more precise estimation of the SLP, reducing the impact of random fluctuations. The resulting values under the same conditions were then combined into a single representative value through a weighted average, defined as:

$$\bar{S} = \frac{\sum_{i=1}^{N} w_i S_i}{\sum_{i=1}^{N} w_i}, \quad \text{where } w_i = \frac{1}{\sigma_i(S_i)^2} \qquad (7)$$

The corresponding Type A uncertainty (from the weighted average) was given by

$$\sigma_{\bar{S},A} = \sqrt{\frac{1}{\sum_{i=1}^{N} w_i}} \qquad (8)$$

To account for the variability among individual data sets, arising from possible sources such as temperature fluctuations, an additional contribution to the uncertainty was included. In particular, we introduced a Type B uncertainty associated with the ambiguity in selecting the exact peak. In practice, the maximum temperature is not reached at a single point but rather over a short plateau of several points with nearly identical values, determined by the resolution of the temperature probe (see SI, section 1, for an illustrative example). This feature makes the precise identification of the peak ambiguous. To quantify this effect, for each temperature

curve i, two values of S were computed: S_i^{first}, obtained by taking the first data point that reaches the maximum temperature, and S_i^{last}, obtained by taking the last data point at that same temperature. The Type B contribution for curve i was then defined as

$$\sigma_{S_i,\text{B}} = \frac{\left| S_i^{\text{First Max}} - S_i^{\text{Last Max}} \right|}{2} \tag{9}$$

and the overall Type B uncertainty was obtained by averaging over all curves:

$$\sigma_{\bar{S},\text{B}} = \frac{1}{N} \sum_{i=1}^{N} \sigma_{S_i,\text{B}} \tag{10}$$

Finally, the combined uncertainty at each point was obtained by combining both contributions:

$$\sigma_{\bar{S},\text{C}} = \sqrt{\sigma_{\bar{S},\text{A}}^2 + \sigma_{\bar{S},\text{B}}^2} \tag{11}$$

where $\sigma_{\bar{S},\text{A}}$ is the Type A (statistical) uncertainty. Note that $\sigma_{\bar{S},\text{B}}$ is included only for the PAM-derived results, whereas a much larger such type of uncertainty is likely to be present for the ISM regarding the starting "time zero" point. Consider, for example, the change in concavity often observed (see *e.g.* ref. 16–29): where would the 0-time would be set for such measurements? SI Fig. 1(b) illustrates this point. We did not consider such Type B uncertainty for the ISM, however, because it is not the objective of the current work, and it is only shown for completeness.

3. Results and discussion

3.1. Effect of the number of fitted points on the SLP value

In our study, we repeated the measurement of a single batch of particles 30 times, always starting at a very similar temperature. These measurements were grouped into 3 sets of 10 measurements within which the alternating magnetic field was applied for varying amounts of time (1, 2 and 4 min). The idea of applying the alternating magnetic field for different times was to investigate if there was any effect of the different curvature at the peak on the SLP values calculated with the PAM.

Each of the measurements was analyzed using the PAM, following the procedure described above. Since the ISM is still one of the most widely employed calorimetric approaches to determine the SLP in experimental practice, we also included its analysis for the sake of completeness, providing us a direct comparison between both methods. For clarity, Fig. 1 provides a schematic representation of the systematic procedure followed in both approaches. Panel (a) shows the heat and cool curve, where the time intervals selected for the analysis are highlighted, while panels (b) and (c) depict the SLP values obtained using the PAM and ISM methods, respectively, as a function of the considered time windows. In general, Fig. 1 shows a large uncertainty on the determined SLP value over the first seconds of measurement, which decreases rapidly
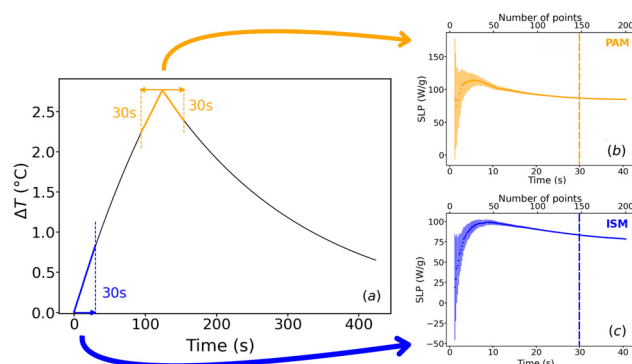

Fig. 1 Experimental SLP determination using both ISM (blue) and PAM (orange) methods. Panel (a) shows the temperature rise curve with the selected time intervals for each analysis, while panels (b) and (c) display the corresponding SLP values as a function of the analyzed time window.

after 10 seconds. It is also noted an overall higher SLP value obtained through the PAM approach over that obtained from the ISM, an aspect that will be further discussed later. The vertical dashed lines denote a 30-second interval, commonly adopted in experimental practice.

The results displayed in Fig. 1 show, both for the PAM and ISM approaches, a marked dependence of the determined SLP value on the number of data points analysed. This is in agreement with previous reports indicating that the arbitrary determination of the linear range used for the SLP calculations may lead to inaccurate values.[30] Although some authors perform SLP calculations with a specific analysis of the time interval used for the SLP calculation,[31] in many other cases the time interval for the analysis is generally either not reported or arbitrarily selected. For this reason, we implemented our proposed statistical analysis to establish the range in which the linear fit should be applied for each measurement, both in the ISM and in the PAM analysis. In the following we will analyse the dependence of the SLP value on the selected time range for linear fit, and consequently on the number of data points considered.

3.2. Linear-range identification for SLP determination

Before showing the results of the complete data set, which consisted of several repetitions for each case, we first present a detailed description of the analysis procedure using a single, arbitrary $\Delta T(t)$ curve as an example.

3.2.1. Single measurement. To determine with precision the linear range of the $\Delta T(t)$ curves we employed the well-established F-test, described in detail in section 2.4, which allows to assess whether the inclusion of an additional parameter (transforming the model from linear to quadratic) provides a statistically significant improvement in the fit. For those readers interested in a more intuitive meaning of the F-test to distinguish linear behaviour, in the SI, section 2, it is shown in correspondence with the root mean square errors (RMSE) of the linear and quadratic fits.
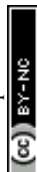
Fig. 2(a) and (b) show the SLP values as a function of the number of points considered in the fits, using the PAM and the ISM. In both cases, the shaded regions mark the time intervals where extending the fit from the origin results in the optimal linear fit according to the *F*-test, minimizing the errors associated with the use of a smaller time range. This representation makes it evident that the region in which the linear approximation is statistically justified lies far from the range that is most commonly adopted in the literature, typically around 30 seconds (see, *e.g.*, ref. 2, 32 and 33 or even larger time ranges[34]). Indeed, for this particular measurement, the SLP value determined from the ISM using the first 30 s for the fit was 83.4 W g^{-1} while using the optimum range was 97.5 W g^{-1}, resulting in a 17% difference. When using the PAM for the SLP determination, the obtained values were 87.0 W g^{-1} using 30 s for the fit and 112.2 W g^{-1} for the optimum value determined using the time range determined from the statistical analysis. This comparison clearly illustrates the risk of underestimating or overestimating the SLP when the data are analysed without an objective determination of the linear range. We also note that the PAM method gives a higher value as found in ref. 6 because it compensates for the heat loss

thereby approximating adiabatic conditions. It is worth to recall that in this particular measurement, the linear range of the PAM approach occurs at a shorter time range that the ISM one. It will be interesting to check whether the same trend is maintained for other measurements.

3.2.2. Repeated measurements. We move now from the analysis of a single measurement to the consideration of repeated measurements for each of the experimental conditions studied, as already introduced in the previous section.

Fig. 3 shows the results of the 30 measurements in which the temperature *versus* time data have been normalized to highlight the relative temperature variation throughout the experiment. This normalization was performed to facilitate the comparison of the results, as there were slight differences in the initial temperature conditions at the start of each experimental run. As can be observed in the figure, variations appear between different repetitions. Since there was no systematic variation with the order in which they were taken, these differences can be attributed to random fluctuations, highlighting the importance of averaging repeated measurements. Several factors can contribute to these differences, such as small variations in the starting temperature (see SI, section 3) or the presence of initial thermal drift (if the system temperature had not fully stabilized before starting the field application, even small drifts could propagate into noticeable differences at short heating times). These differences highlight the difficulty to obtain reproducible experimental results in the SLP determination through calorimetric methods. It is worth mentioning that all the measurements were performed starting at a very similar temperature and therefore, the possible differences associated to measurement at different temperatures, as reported elsewhere[35,36] would be minimal (see Fig. 3 within the SI).

Focusing on a single time interval for the AC field application, Fig. 4(a) and (b) show the SLP values obtained from ten independent measurements performed under a 2-minute
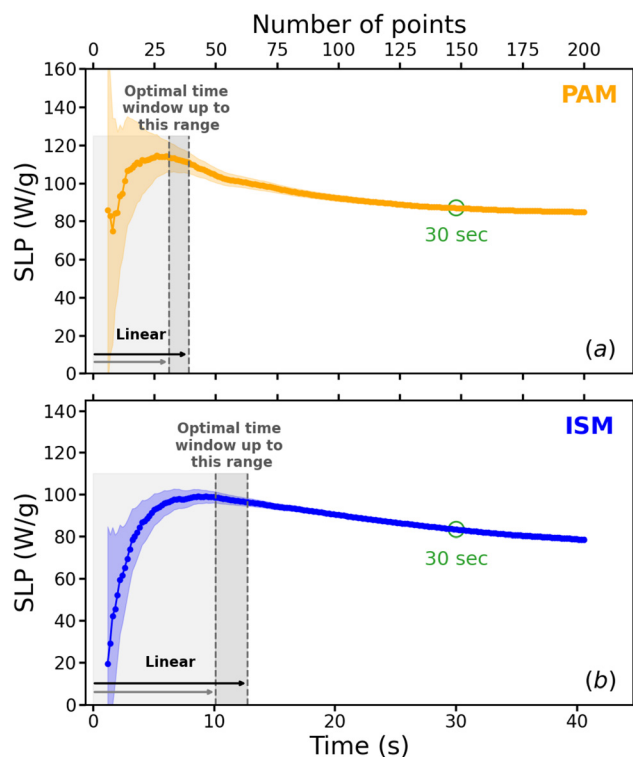

Fig. 2 SLP values obtained with the Peak Analysis Method (PAM, (a)) and the Initial Slope Method (ISM, (b)) as a function of number of points/time. Shaded regions represent propagated uncertainties, and horizontal arrows indicate the smallest (light gray) and largest (black) temporal range used for the linear fits, that the *F*-test classifies as linear. Obtained from the beginning of the heating stage (ISM) or from the peak toward both sides (PAM), the optimal time window is displayed as a vertical band in both cases, where the *F*-test condition ($F < F_{crit}$) is satisfied. The green circle indicates the SLP value at 30 s for reference.
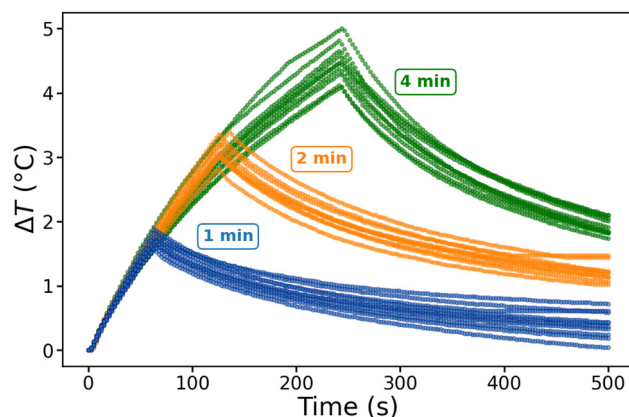

Fig. 3 Temperature variation over time in calorimetry experiments for SLP determination. Bottom, middle and top datasets correspond to applying field times of 1, 2 and 4 min, respectively. Results correspond to 10 independent measurements of the same particles.
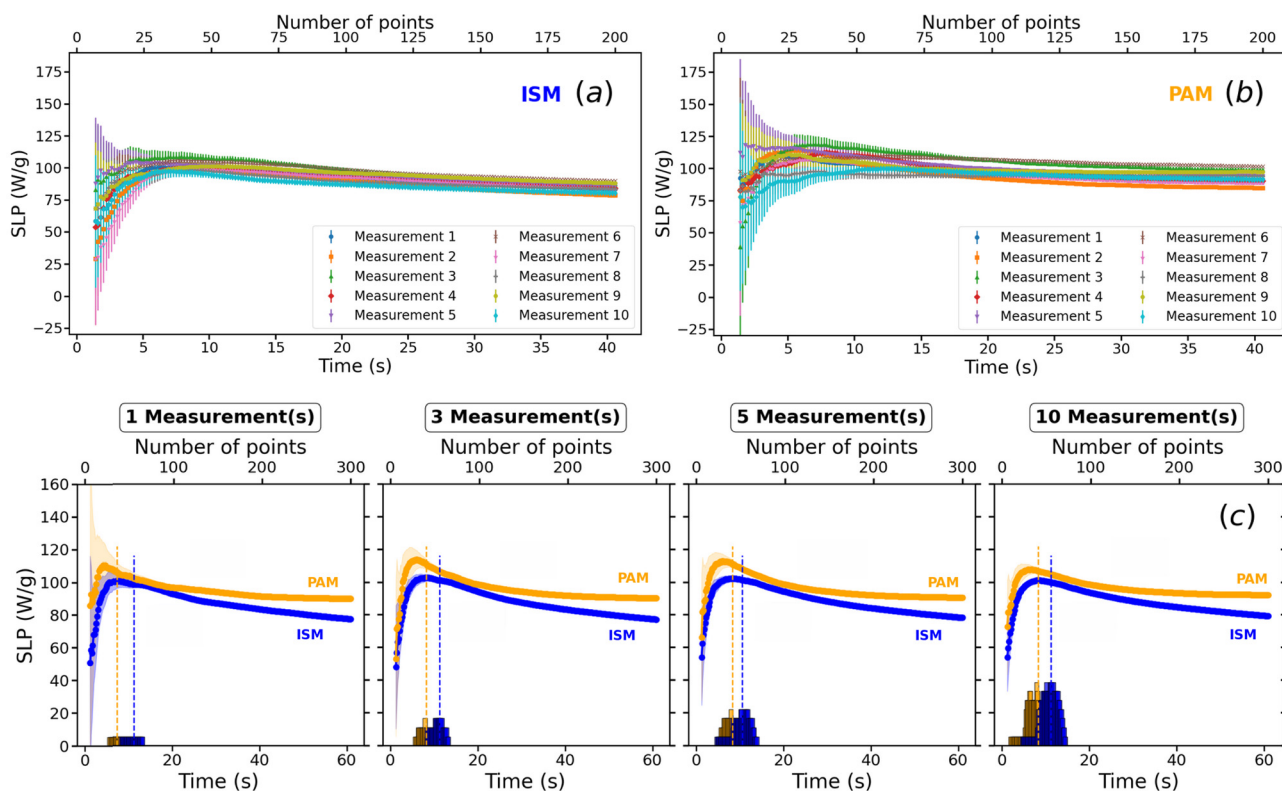
Fig. 4 Analysis of repeated measurements. (Top panels) SLP values obtained from each of the ten independent measurements using the ISM (a) and PAM (b) for a heating time of 2 minutes. (Bottom panels) (c) Evolution of the averaged SLP values as the number of measurements considered increases (from 1 to 10), for both the ISM and PAM approaches. The histograms displayed at the bottom of each panel represent the distribution of the linear ranges determined by the F-test ($F < F_{crit}$), with vertical dotted lines indicating the average optimal time window obtained from this criterion.

applied field. As can be seen, variations arise between the SLP values calculated from the individual measurements, which could be related to small drifts in the initial temperature, as already discussed above. The observed variability between measurements requires the individual determination of the optimal temperature range for accurate SLP assessment. Once the individual SLP values are obtained, to reduce uncertainty, results from up the ten individual measurements need to be combined.

The lower panels of Fig. 4 illustrate how the SLP values evolve as the number of repeated measurements included in the analysis increases, for both the ISM and PAM approaches. The histograms displayed at the bottom of each panel represent the distribution of the linear ranges determined by the F-test for the different measurements considered. The average SLP values were calculated using the weighting procedure and the uncertainty definitions presented in section 2.4. It is clearly observed that increasing the number of measurements reduces the uncertainty of the results, since a larger statistical sample provides a more precise estimate of the SLP. For example, the SLP value determined from the ISM using the first measurement was 98.6 ± 2.3 W g^{-1} while the SLP obtained from ten measurements was 99.5 ± 0.7 W g^{-1}. in the case of the PAM, the obtained values were 107.3 ± 7.1 W g^{-1} for the

first measurement and 106.7 ± 2.1 W g^{-1} for combined results of ten measurements. These results clearly validate the use of repeated measurements to reduce the uncertainty in the SLP determination.

3.2.3. Differences between the ISM and PAM approaches. From the results depicted in Fig. 4, it is also important to note that the ISM systematically underestimates the SLP values compared to those obtained with the PAM. Indeed, the blue line corresponding to the SLP values obtained from the ISM is always below the one corresponding for those obtained through the PAM analysis (see Fig. 4(c)). This behaviour is consistent with previous reports in the literature,[37] and highlights the relevance of using an approach such as PAM, which minimizes the bias introduced by the assumptions inherent to Newton-law-based analyses. We note here that Newton's law of cooling is applicable only to losses from a sample with a uniform temperature,[5,6] which is rarely the case in practice.[2,3] The limitations associated with the initial slope method have been extensively discussed in the literature, highlighting several critical challenges that affect its reliability and applicability.[6,30,38] To solve this, other data analysis approaches have been proposed (*e.g.*, the Box Lucas method,[34] the corrected slope method[39] or the stepped heating procedure[40]).

However, it is important to highlight here the problems associated with the assumption of linear heat losses. The general scenario for SLP determination may be summarised as follows: once the AC field is switched on, the particles start releasing heat. At this initial stage, the SLP value could be obtained from the linear slope of the $\Delta T(t)$ curve, the ISM. However this assumes ideal adiabatic behaviour, whereas as soon as the system temperature differs from that of the environment, there is a flux of energy to the environment. Such heat loss is often assumed to be linear and described by the so-called Box–Lucas equation, of the form:

$$T(t) = T_{\text{env}} + \frac{S}{a}[1 - e^{-at}], \tag{12}$$

with T_{env} the temperature of the environment, and S related to the SLP as indicated in eqn (5).

Note that $S = \lim_{t \to 0} \frac{dT}{dt}$, corresponding to the ISM limit. It is also worth noting that eqn (12) corresponds to the scenario sometimes referred to as Newton's law of cooling, as the rate of heat losses is proportional to the difference in temperatures between sample and environment.[4] However, as stated earlier, this only applies in the case of a uniformly heated medium.

In practice, this linear loss assumption is very limited, restricted to the very first stages of the heating process, corresponding to small temperature differences. Over time, non-uniform sample temperature profiles,[2,3] compounded by the coexistence of several heat loss mechanisms, lead to strong nonlinear losses and eqn (12) becomes inapplicable. The increasing non-uniformity of the temperature profile is illustrated in Fig. 5(a), where a typical laboratory measurement has been reproduced using finite-element simulations in COMSOL Multiphysics® (see SI, section 4 for details). Generally, the assumption of a homogeneous temperature within the sample is not the case in practice. These problems have been thoroughly discussed by Wildeboer et al.[39]

It is in this context that the PAM approach demonstrates unmatched strength compared to methods based on Newton's Law of Cooling. As outlined in section 2.3, its advantage lies in the fact that it is independent of the actual temperature profiles, as far as they are sufficiently similar. And, as discussed in detail in Ruta et al.,[6] that happens close to the peak of the $\Delta T(t)$ curve, at the switch on/off transition. This is illustrated in Fig. 5(b), where it is shown the typical $\Delta T(t)$ curve corresponding to the simulated sample in panel (a): the insets in Fig. 5(b) clearly show that the temperature profiles are much more similar close to the peak. These results are consistent with those reported in our previous work,[6] but extending the 1D model used there to a more complete 3D case. To complete the analysis, it is worth recalling here that the linear -or non-linear- character of the experiment can be determined[6,41] by plotting the time derivative of the $\Delta T(t)$ curve, $d(\Delta(T))/dt$, against $\Delta(T)$, as illustrated schematically in Fig. 5(c).

The conclusion of the above arguments is that approaches based on the so-called Newton's law of cooling are, in general, inadequate to describe and analyse experimental data. While
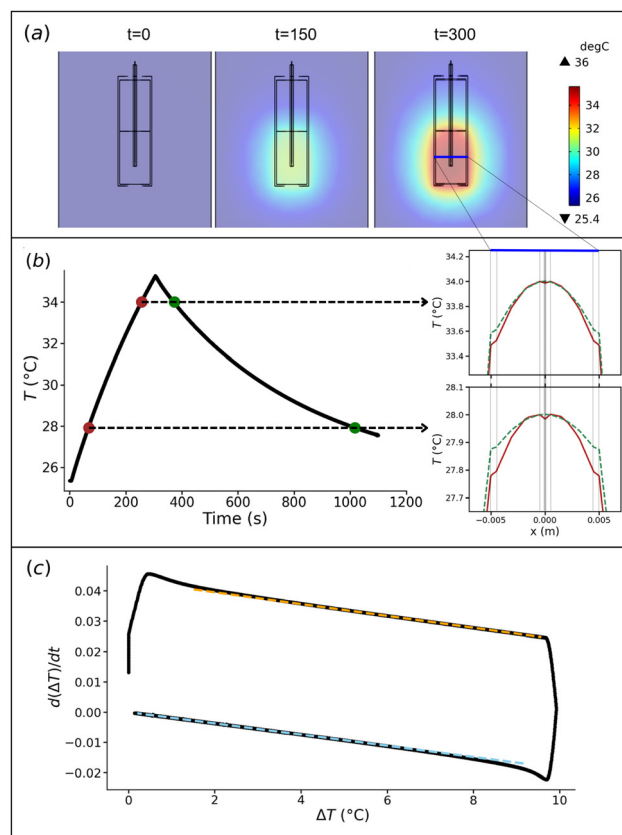

Fig. 5 Schematic representation of the main limitations in SLP determination. (a) Temperature colormap from COMSOL simulations at selected times. (b) Temporal evolution of the temperature; the subplots show differences in the temperature gradient. (c) Nonlinear character of the system evidenced by plotting the derivative d(ΔT)/dt against ΔT, which deviates from the simple linear loss assumption.

in general these difficulties are known in the related literature, all models to determine the heating power of the nanoparticles are based on such type of approaches (including others, such as the corrected-slope method[39]). Our objective in ref. 6 was to go beyond this type of approaches, into a more physically realistic scenario. Although not important for the above discussion, it is worth noting that the simulations also yield larger SLP values for the PAM approach compared with the ISM, consistent with the experimental observations (see SI, section 5).

3.3. Comparison among different measurements and time intervals

Following the analysis based on a single time interval for the AC field application, we now examine the potential influence of the field application time on the SLP measurement, particularly in terms of the slope variations observed during peak analysis. Therefore, as stated earlier, we conducted a series of measurements at different time intervals to assess the potential impact of field exposure duration on the SLP determination. Specifically, we compare the average SLP values obtained for different heating times (1, 2, and 4 minutes) using the same batch of particles. The analysis includes the
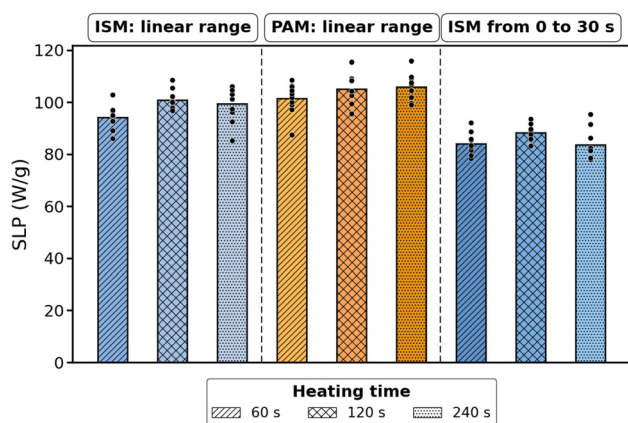
Fig. 6 Average SLP values for different heating times (60, 120, and 240 s), obtained using the ISM and PAM methods by fitting the slopes within the objectively determined linear range of the heating and cooling branches, as well as the ISM applied to the first 30 seconds of heating. Results corresponding to each independent measurement are also shown.

SLP values determined with the ISM by fitting the temperature rise during the first 30 seconds of heating, which is a commonly adopted practice in the literature, and those obtained with both ISM and PAM by fitting the slopes within the objectively determined linear range of the heating and cooling branches (Note that the ISM used here has not considered any further correction including the thermal losses such as the corrected-slope method or Box-Lucas method). In the latter cases, the reported SLP values correspond to the averages of the histograms within those linear intervals. The results are summarized in Fig. 6.

As discussed in the previous section, it can be clearly observed that the SLP values obtained with the ISM are systematically lower than those derived using the PAM. This is consistent with the intrinsic underestimation of SLP by the ISM due to its neglect of some loss mechanisms in the system and its assumption of Newton's law of cooling. A particularly interesting feature is the significant difference between the SLP values obtained in the determined linear range (both for ISM and PAM) and those derived from the ISM when restricted to the first 30 seconds of heating, as is commonly done in experimental practice. As also mentioned in the previous section, this observation highlights the limitations of such a conventional approach and underlines the importance of employing objective criteria, such as the F-test, to identify the linear range and avoid systematic errors in the determination of the SLP.

4. Development of a web-based software for SLP calculation

We are aware that the methodology proposed for SLP calculation based on the F-test analysis entails a degree of complex-

ity that may hinder its implementation. Therefore, to address this challenge and promote greater accessibility, we have developed a dedicated software tool that facilitates the execution of this type of analysis in a more streamlined and user-friendly manner.

The software, built in Python, provides an interactive interface that guides the user through the complete workflow, from data loading to the calculation of Specific Loss Power (SLP). The application can be found at SLPCalculator.com. Upon starting the analysis, the program prompts the user to provide the input data, which can be provided in different formats, always specifying the columns corresponding to time and temperature. The sampling interval is then automatically calculated, and the imported data are displayed for verification, with the option to save the graphical representation of the datasets.

Before performing the SLP calculations, the program requires input of the key physical parameters of the system under study, including the density and specific heat of the magnetic nanoparticles and of the carrier fluid, as well as the particle concentration. The program then integrates the two complementary approaches described in this work: the PAM and the ISM. For each dataset, it applies the statistical criterion based on the F-test presented in this article and calculates the corresponding values together with their associated uncertainties. The results are displayed graphically, including confidence bands and visual indicators that highlight the optimal window sizes.

The software has been designed to be modular, ensuring readability. Its simple interface makes the analysis accessible even to users without programming experience. We think that this custom software will ensure consistency, while providing a user-friendly workflow to obtain SLP values from experimental data and to standardize their determination, thus facilitating comparisons and reproducibility among different research groups.

5. Conclusions

In this work, based on our previous study in which we introduced the Peak Analysis Method (PAM) as an alternative to conventional approaches based on Newton's law of cooling,[6] we have developed a statistical framework to define with precision the linear applicability range of PAM, as well as other methods based on linear fitting procedures. For this purpose, we have implemented the F-test of the additional parameter, which provides an objective criterion to discriminate between linear and non-linear regimes.

Our results show that the linear range obtained through this analysis is significantly different from the time windows commonly assumed in experimental practice. This explains, at least in part, the large variability in reported SLP values across different laboratories when Newton's-cooling-law-based methods are employed without a statistical analysis.

Finally, as a major outcome of this study, we have developed a web-based application that implements PAM in combination with the *F*-test. The code also makes a comparison with the ISM, which is generally found to give artificially low values of SLP due to the associated neglect of heat losses. This tool enables researchers to determine the SLP (or SAR) in a systematic and reproducible manner, without the need for subjective or manual fitting procedures. By minimizing the variability and bias associated with conventional analyses, this general approach paves the way toward more reliable and comparable SLP determinations in the magnetic hyperthermia and photothermal heating communities.

Author contributions

Iago López-Vázquez: Conceptualization; formal analysis; investigation; validation; visualization; writing – original draft. Yilian Fernández-Afonso: Formal analysis; investigation; writing – review and editing. Antonio Santana-Otero: Investigation; writing – review and editing. Sergiu Ruta: Conceptualization; writing – review and editing. Alfredo Amigo: Conceptualization; writing – review and editing. M. Puerto Morales: Funding acquisition; writing – review and editing. Roy W. Chantrell: Conceptualization; methodology; supervision; writing – original draft. Lucía Gutiérrez: Conceptualization; funding acquisition; visualization; writing – original draft. David Serantes: Conceptualization; funding acquisition; methodology; supervision; visualization; writing – original draft.

Conflicts of interest

Authors declare no conflicts of interest.

Data availability

Data for this article, including all experimental and theoretical datasets are available at ZENODO at https://doi.org/10.5281/zenodo.17709500.

SLPCalculator is free to use and available at: https://slpcalculator.com/.

Supplementary information (SI) is available. Supplementary information includes: 1) Illustration of Type B uncertainty sources, 2) RMSE as an intuitive complement to the F-test, 3) Initial Temperature variations, 4) Description of finite-element simulations, 5) SLP COMSOL-simulated values. See DOI: https://doi.org/10.1039/d5nr04995d.

Acknowledgements

References

1 J. Wells, D. Ortega, U. Steinhoff, S. Dutz, E. Garaio, O. Sandre, E. Natividad, M. M. Cruz, F. Brero, P. Southern, *et al.*, *Int. J. Hyperthermia*, 2021, **38**, 447–460.

2 A. Espinosa, J. Kolosnjaj-Tabi, A. Abou-Hassan, A. Plan Sangnier, A. Curcio, A. K. Silva, R. Di Corato, S. Neveu, T. Pellegrino, L. M. Liz-Marzán, *et al.*, *Adv. Funct. Mater.*, 2018, **28**, 1803660.

3 D. Valdés, T. Torres, A. M. Maldonado, G. Urretavizcaya, M. Nadal, M. V. Mansilla, R. Zysler, G. Goya, E. De Biasi and E. Lima Jr, *Phys. Rev. Appl.*, 2023, **19**, 014042.

4 G. Landi, *J. Magn. Magn. Mater.*, 2013, **326**, 14–21.

5 M. Vollmer, *Eur. J. Phys.*, 2009, **30**, 1063.

6 S. Ruta, Y. Fernández-Afonso, S. E. Rannala, M. P. Morales, S. Veintemillas-Verdaguer, C. Jones, L. Gutiérrez, R. W. Chantrell and D. Serantes, *Nanoscale Adv.*, 2024, **6**, 4207–4218.

7 Y. Fernández-Afonso, S. Ruta, A. Páez-Rodríguez, T. S. van Zanten, S. Gleadhall, R. M. Fratila, M. Moros, M. D. P. Morales, A. Satoh, R. W. Chantrell, *et al.*, *Adv. Funct. Mater.*, 2024, 2405334.

8 I. Morales, R. Costo, N. Mille, J. Carrey, A. Hernando and P. de la Presa, *Nanoscale Adv.*, 2021, **3**, 5801–5812.

9 N. Mille, D. De Masi, S. Faure, J. M. Asensio, B. Chaudret and J. Carrey, *Appl. Phys. Lett.*, 2021, **119**, 022407.

10 H. Gavilán, K. Simeonidis, E. Myrovali, E. Mazarío, O. Chubykalo-Fesenko, R. Chantrell, L. Balcells, M. Angelakeris, M. P. Morales and D. Serantes, *Nanoscale*, 2021, **13**, 15631–15646.

11 M. A. Vergés, R. Costo, A. Roca, J. Marco, G. Goya, C. Serna and M. D. P. Morales, *J. Phys. D: Appl. Phys.*, 2008, **41**, 134003.

12 J. Teller, F. Westphal and C. Gruettner, Magnetic nanoparticles having improved magnetic properties, *US Patent* 7691285, 2010.

13 C. C. Scarneciu, L. Sangeorzan, H. Rus, V. D. Scarneciu, M. S. Varciu, O. Andreescu and I. Scarneciu, *Pak. J. Med. Sci.*, 2017, **33**, 111.

14 A. DeLean, P. J. Munson and D. Rodbard, *Am. J. Physiol.: Endocrinol. Metab.*, 1978, **235**, E97.

15 P. R. Bevington and D. K. Robinson, *Data reduction and error analysis for the physical sciences*, McGraw-Hill, New York, NY, 3rd edn, 2003.

16 C. Chen, P. Wang, H. Chen, X. Wang, M. N. Halgamuge, C. Chen and T. Song, *ACS Appl. Mater. Interfaces*, 2022, **14**, 14049–14058.

17 V. Aquino, M. Vinícius-Araújo, N. Shrivastava, M. Sousa, J. Coaquira and A. Bakuzis, *J. Phys. Chem. C*, 2019, **123**, 27725–27734.

18 S. F. Shams, M. R. Ghazanfari, S. Pettinger, A. H. Tavabi, K. Siemensmeyer, A. Smekhova, R. E. Dunin-Borkowski, G. G. Westmeyer and C. Schmitz-Antoniak, *Phys. Chem. Chem. Phys.*, 2020, **22**, 26728–26741.

19 T. M. Elkhova, Y. K. Gun'ko, A. P. Pyatakov, Y. I. Spichkin, K. Dawson and A. M. Tishin, *Solid State Phenomena*, 2014, **215**, 454–458.

20 S. B. Attanayake, M. D. Nguyen, A. Chanda, J. Alonso, I. Orue, T. R. Lee, H. Srikanth and M.-H. Phan, *ACS Appl. Mater. Interfaces*, 2025, **17**, 19436–19445.

21 F. Reyes-Ortega, B. L. Checa Fernández, A. V. Delgado and G. R. Iglesias, *Pharmaceutics*, 2019, **11**, 517.

22 D. Durneata, R. Hempelmann, O. Caltun and I. Dumitru, *IEEE Trans. Magn.*, 2014, **50**, 1–4.

23 F. Hirosawa and T. Iwasaki, *Solid State Sci.*, 2021, **118**, 106655.

24 J. Kurian, B. Lahiri, M. J. Mathew and J. Philip, *J. Magn. Magn. Mater.*, 2021, **538**, 168233.

25 X. L. Liu, E. S. G. Choo, A. S. Ahmed, L. Y. Zhao, Y. Yang, R. V. Ramanujan, J. M. Xue, D. Di Fan, H. M. Fan and J. Ding, *J. Mater. Chem. B*, 2014, **2**, 120–128.

26 A. Chalkidou, K. Simeonidis, M. Angelakeris, T. Samaras, C. Martinez-Boubeta, L. Balcells, K. Papazisis, C. Dendrinou-Samara and O. Kalogirou, *J. Magn. Magn. Mater.*, 2011, **323**, 775–780.

27 D. Mondal, G. Phukan, N. Paul and J. Borah, *J. Magn. Magn. Mater.*, 2021, **528**, 167809.

28 P. De La Presa, Y. Luengo, V. Velasco, M. Morales, M. Iglesias, S. Veintemillas-Verdaguer, P. Crespo and A. Hernando, *J. Phys. Chem. C*, 2015, **119**, 11022–11030.

29 I. Craciunescu, P. Palade, N. Iacob, G. M. Ispas, A. E. Stanciu, V. Kuncser and R. P. Turcu, *J. Phys. Chem. C*, 2021, **125**, 11132–11146.

30 H. L. Ring, A. Sharma, R. Ivkov and J. C. Bischof, *Int. J. Hyperthermia*, 2020, **37**, 100–107.

31 D. E. Bordelon, C. Cornejo, C. Grüttner, F. Westphal, T. L. DeWeese and R. Ivkov, *J. Appl. Phys.*, 2011, **109**, 124904.

32 C. Papadopoulos, E. K. Efthimiadou, M. Pissas, D. Fuentes, N. Boukos, V. Psycharis, G. Kordas, V. C. Loukopoulos and G. C. Kagadis, *Phys. Med.*, 2020, **71**, 39–52.

33 D. Egea-Benavente, C. Díaz-Ufano, Á. Gallo-Cordova, F. J. Palomares, J. L. Cuya Huaman, D. F. Barber, M. D. P. Morales and J. Balachandran, *ACS Appl. Mater. Interfaces*, 2023, **15**, 32162–32176.

34 O. L. Lanier, O. I. Korotych, A. G. Monsalve, D. Wable, S. Savliwala, N. W. Grooms, C. Nacea, O. R. Tuitt and J. Dobson, *Int. J. Hyperthermia*, 2019, **36**, 686–700.

35 I. Andreu, E. Natividad, L. Solozabal and O. Roubeau, *J. Magn. Magn. Mater.*, 2015, **380**, 341–346.

36 E. Garaio, J.-M. Collantes, J. A. Garcia, F. Plazaola and O. Sandre, *Appl. Phys. Lett.*, 2015, **107**, 123103.

37 E. A. Perigo, G. Hemery, O. Sandre, D. Ortega, E. Garaio, F. Plazaola and F. J. Teran, *Appl. Phys. Rev.*, 2015, **2**, 041302.

38 A. Makridis, S. Curto, G. Van Rhoon, T. Samaras and M. Angelakeris, *J. Phys. D: Appl. Phys.*, 2019, **52**, 255001.

39 R. R. Wildeboer, P. Southern and Q. A. Pankhurst, *J. Phys. D: Appl. Phys.*, 2014, **47**, 495003.

40 N. Iacob, G. Schinteie, P. Palade, C. Ticos and V. Kuncser, *Eur. Phys. J. E: Soft Matter Biol. Phys.*, 2015, **38**, 57.

41 L. G. Hanson, B. L. Hansen, T. Veile, M. Zambach, N. B. Christensen and C. Frandsen, *IEEE Magn. Lett.*, 2023, **14**, 1–5.